energies

MDPI

Article

Sizing and Coordination Strategies of Battery Energy Storage System Co-Located with Wind Farm: The UK Perspective

Fulin Fan [1,*], Giorgio Zorzi [1], David Campos-Gaona [1], Graeme Burt [1], Olimpo Anaya-Lara [1], John Nwobu [2] and Ander Madariaga [2]

[1] Department of Electronic and Electrical Engineering, University of Strathclyde, Glasgow G1 1XW, UK; giorgio.zorzi@strath.ac.uk (G.Z.); d.campos-gaona@strath.ac.uk (D.C.-G.); graeme.burt@strath.ac.uk (G.B.); olimpo.anaya-lara@strath.ac.uk (O.A.-L.)

[2] Offshore Renewable Energy Catapult, Glasgow G1 1RD, UK; john.nwobu@ore.catapult.org.uk (J.N.); ander.madariaga@ore.catapult.org.uk (A.M.)

* Correspondence: f.fan@strath.ac.uk

Abstract: The rapid development and growth of battery storage have heightened an interest in the co-location of battery energy storage systems (BESS) with renewable energy projects which enables the stacking of multiple revenue streams while reducing connection charges of BESS. To help wind energy industries better understand the coordinated operation of BESS and wind farms and its associated profits, this paper develops a simulation model to implement a number of coordination strategies where the BESS supplies enhanced frequency response (EFR) service and enables the time shift of wind generation based on the UK perspective. The proposed model also simulates the degradation of Lithium-Ion battery and incorporates a state of charge (SOC) dependent limit on the charge rate derived from a constant current-constant voltage charging profile. In addition, a particle swarm optimisation-based battery sizing algorithm is developed here on the basis of the simulation model to determine the optimal size of the co-located BESS along with SOC-related strategy variables that maximise the net present value of the wind + BESS system at the end of the EFR contract.

Keywords: battery energy storage system; co-located system; coordination strategy; frequency response; particle swarm optimisation

Citation: Fan, F.; Zorzi, G.; Campos-Gaona, D.; Burt, G.; Anaya-Lara, O.; Nwobu, J.; Madariaga, A. Sizing and Coordination Strategies of Battery Energy Storage System Co-Located with Wind Farm: The UK Perspective. *Energies* **2021**, *14*, 1439. https://doi.org/10.3390/en14051439

Academic Editor: Teuvo Suntio

Received: 16 February 2021
Accepted: 4 March 2021
Published: 6 March 2021

Publisher's Note: MDPI stays neutral with regard to jurisdictional claims in published maps and institutional affiliations.

Copyright: © 2021 by the authors. Licensee MDPI, Basel, Switzerland. This article is an open access article distributed under the terms and conditions of the Creative Commons Attribution (CC BY) license (http://creativecommons.org/licenses/by/4.0/).

1. Introduction

Battery energy storage systems (BESS) play an important role in the transition to a low-carbon electricity generation, offering great potential for improving the system flexibility and facilitating the integration of renewables [1]. A BESS can assist in the time shift of renewable generation [2], reduce the need for network reinforcement [3], provide ancillary services to the grid [4,5], and exploit arbitrage opportunities from electricity price differentials [6]. While the BESS offer potential benefits in many parts of the grid, their synergies with renewable energy is an increasingly attractive option in the UK. The BESS co-located with renewable power plants can help project developers manage the intermittent nature of renewables and/or stack multiple revenue streams such as frequency response (FR) services [7].

In order to maintain the grid frequency closer to 50 Hz in GB, the National Grid Electricity System Operator (NGESO) has introduced a range of FR services to balance generation and demand. These services are achieved either through the mandatory requirement where transmission-connected generators may be asked to offer mandatory FR, or through a commercial arrangement such as firm FR (FFR) and enhanced FR (EFR) [8]. FFR services are procured on a monthly basis and can provide both dynamic and non-dynamic responses to changes in frequency; dynamic FR is a continuously provided service used to manage the normal second-by-second changes on the system, while non-dynamic FR

is typically a discrete service triggered at a defined frequency deviation [9]. Delivering FFR by a BESS can pose challenges in managing the state of charge (SOC) of the BESS. To deal with this issue, the BESS providers in the GB are suggested either (i) to keep spare, uncontracted capacity of the BESS which can then be used for the SOC management, or (ii) to use the BESS as part of mixed technology assets so that the FFR can be delivered by other assets while the SOC is restored to an acceptable level [10]. The NGESO, as an alternative to procuring increasing volumes of FR, introduced in 2016 an EFR service which, by responding faster than existing FR services, helps reduce the increasing response required at times of low system inertia [11]. Given the nature of the EFR service which allows storage technologies to manage their SOC, 61 of the 64 sites in the first EFR tender round were storage based, and all of the eight successful tenders used Lithium-Ion BESS to provide a combined 201 MW of EFR for 4 years with an average price of GBP 9.44/MW of EFR/hr [11]. During the transition to a new suite of dynamic FR services (i.e., Dynamic Containment, Dynamic Moderation and Dynamic Regulation designed for different ranges of frequency deviations), NGESO launched a 2-year auction trial of Dynamic Low High (DLH) and Low Frequency Static (LFS) services in 2019 so as to test the FR procurement in a weekly pay-as-clear auction [12]. DLH and LFS services are similar to the monthly FFR dynamic and non-dynamic services but procured on a weekly basis, with the DLH requiring equal volume delivery of primary, secondary, and high response [13].

In addition to the provision of FR services, the co-located BESS can store renewable generation which would otherwise be curtailed. When needed, this energy can then be released into the network increasing the revenue associated with renewable energy subsidies. Renewable generators in the GB can benefit from a range of incentive mechanisms including Renewables Obligation (RO) and Contracts for Difference (CFD). The RO scheme works by issuing RO certificates (ROCs) to renewable generators for each MWh of its accredited generation for a 20-year period; ROCs can then be sold to electricity suppliers which need to acquire a specific amount of ROCs so as to meet their obligations [14]. The RO scheme has been closed to new renewable capacity since 2017, following the introduction of the CFD scheme in 2014 which allows the eligible renewable power plants to be paid at a flat rate for their production over a 15-year period [15]. Renewable generators were able to choose between RO and CFD in the transition period during which both schemes were open [14].

The stacking of multiple revenue streams such as a combination of FR payments and renewable energy subsidies could increase the profitability of renewable + BESS systems. In order to optimise the size of the BESS in terms of power (MW) and energy (MWh) for the considered revenue streams, it is necessary to design a suitable coordination strategy for the co-located system. The fluctuating nature of renewable resource translates in limited predictability of renewable power production, leading to an imbalance between bid volumes and actual export. In order to address this imbalance risk using a suitably sized BESS, Ye et al. [16] estimated the rise of the revenue associated with the otherwise curtailed wind generation above the BESS cost for different BESS sizes to form a cost–benefit curve, based on which the best combination of power and energy of BESS was chosen. Korpaas et al. [17] considered daily bids for the energy exchange in the Nordic spot market and operated an energy storage to minimise the imbalance of wind power production, where effects of storage sizes and wind power forecast errors on the annual revenue were assessed. Michiorri et al. [18] found that the optimal power and energy capacity of a BESS increased with the variance and autocorrelation of wind power forecast errors, respectively. Furthermore, some research focuses on the sizing of the BESS which contributes to the system frequency regulation. Liu et al. [19] described an analytical method of sizing an energy storage to improve the grid frequency behaviour. Mejía-Giraldo et al. [20] determined the best size of a BESS that supported Colombian primary frequency regulation service of photovoltaic power plants to minimise the sum of the BESS cost and a penalty specified for an inappropriate SOC causing a risk to FR service. Based on wholesale and FR market prices in GB, Munoz-Vaca [21] assessed the revenue of applying hybrid energy

storage systems for a wind farm and optimised the sizes of supercapacitor and vanadium redox battery used for FR and long-term energy reserve management, respectively.

This paper proposes a UK-based modelling framework to optimise the size of a BESS co-located with an existing wind farm under different coordination strategies where the BESS is used to provide EFR service and capture the wind generation which would otherwise be curtailed due to the limited ampacity of their common connection point. Though the future of EFR is of uncertainty, the EFR is studied here since the strategy developed for the EFR design (i.e., delivering responses within two envelopes) having a higher complexity could be simplified for other dynamic FR services where the response follows a single envelope. Furthermore, the battery degradation and the SOC-dependent operational constraints of a Lithium-Ion BESS are incorporated into the simulation model. After summarising the revenue streams available for a wind + BESS system and the expenses needed to co-locate a BESS with a wind farm in GB, the particle swarm optimisation (PSO) is used in conjunction with the simulation model to determine the BESS size along with the SOC-related strategy variables that maximise the net present value of the system at the end of a 4-year EFR contract.

The paper is structured as follows: Section 2 describes the simulation model of a wind + BESS system, including coordination strategies along with the degradation model and operational limits of the BESS; Section 3 introduces revenues and expenses of the wind + BESS system and the PSO-based sizing algorithm; Section 4 assesses optimisation results and profitability of the co-located system under each strategy; Section 5 presents conclusions and recommendations for further work.

2. Modelling of Wind + BESS System with Coordination Strategy for EFR

2.1. Technical Requirements of EFR Service in the UK

In order to provide enhanced frequency response (EFR), the asset is required to continuously deliver active power to the grid within the upper and lower envelopes (see Figure 1). Two sets of EFR envelopes were designed for wide and narrow deadband services with varying deadband widths [22]. The reference curve which is halfway between the upper and lower envelopes provides a target profile for the assets that do not need the SOC management [22]. Over-delivery or under-delivery of EFR may lead to a deduction in EFR payment which will be described in Section 3.1.1. In addition, the EFR asset must have the ability to deliver at 100% of the EFR capacity P_{EFR}^{cap} for at least 15 min [22]. Since all the eight accepted EFR tenders provided the narrow deadband service [11], Figure 1b is used here to calculate envelopes from the grid frequency.

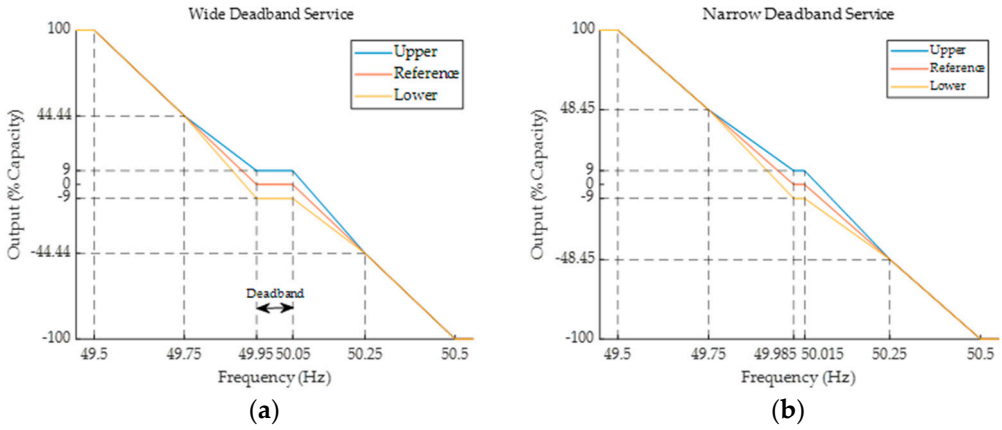

Figure 1. The upper and lower envelopes designed for (**a**) wide and (**b**) narrow enhanced frequency response (EFR) services.

2.2. Modelling of Wind + BESS Systems for EFR

The simulation model developed here calculates the net present value (NPV) of a wind + BESS system based on inputs of grid frequency and available power of wind farm (WF). The grid frequency is first converted into EFR signals comprising the two envelopes and frequency position (i.e., within or outside deadband). Then, a specific coordination strategy dispatches the outputs of BESS and WF based on the SOC of the BESS, EFR signals and available wind power, producing power flows across EFR meter (EFRm) and WF meter (WFm) along with an updated SOC. The variations of SOC within each day are used to model the battery degradation resulting in a reduction of the BESS energy capacity. The readings of EFRm and WFm are then used to calculate the revenue from the EFR provision and the monetary gain/loss of the WF, respectively; the latter is associated with the renewables subsidy of the additional/curtailed wind generation compared to the output of a single WF without a co-located BESS. The EFR payment, gain/loss of WF, and costs of the BESS and its grid connection are discounted to their present values and consequently used to calculate the NPV at the end of a 4-year EFR contract.

2.3. Coordination Strategies of Wind + BESS Systems

Three coordination strategies are developed here for a wind + BESS system: (i) a Non-Power-Exchange (NPE) strategy where the BESS delivers response based on the EFR envelopes and does not exchange energy with the WF, as shown in Figure 2a; (ii) an Enhanced NPE (ENPE) strategy which shares the same configuration with the NPE strategy and reduces the EFR volume within the EFR envelopes to accommodate wind generation; and (iii) a Power-Exchange (PE) strategy where, in addition to the EFR delivery, the BESS interchanges energy with the WF through an additional converter so as to store the otherwise curtailed wind generation due to the limited ampacity of the connection point and discharge the surplus energy to the grid via WFm, as shown in Figure 2b.

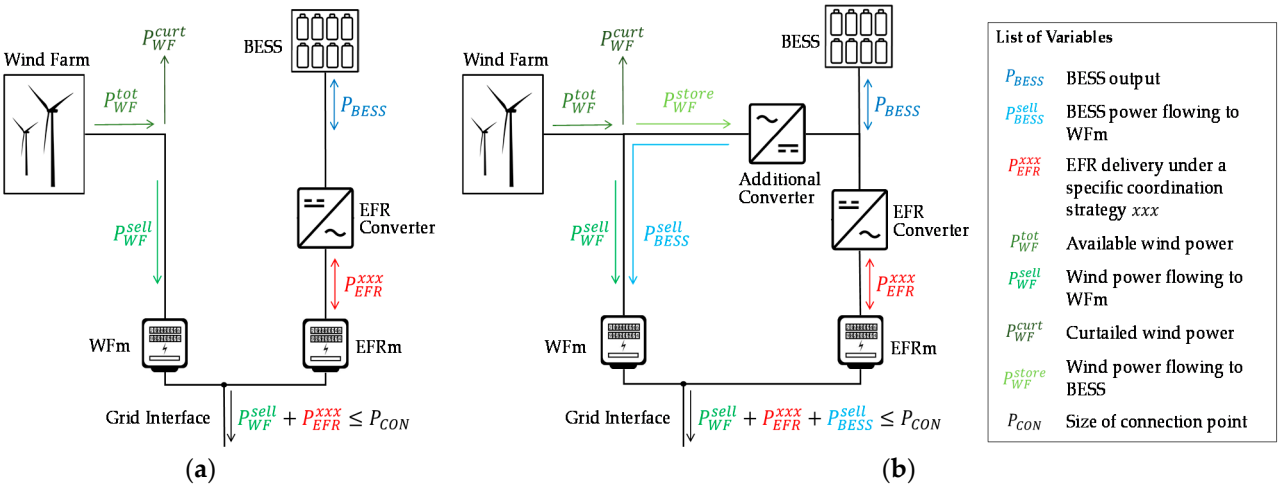

Figure 2. System configurations of (**a**) NPE and ENPE strategies and (**b**) PE coordination strategy.

2.3.1. NPE Coordination Strategy

In the NPE strategy, the BESS output is determined from the EFR envelopes (i.e., higher limits H and lower limits L) by comparing its initial SOC (denoted by SOC_o) with four specific SOC-related variables (i.e., $SOC_{h1} \ge SOC_{h2} \ge SOC_{l2} \ge SOC_{h1}$): (i) given $SOC_o \ge SOC_{h1}$, the BESS only discharges at a positive H; (ii) given $SOC_{h2} \le SOC_o < SOC_{h1}$, the BESS output follows H outside the deadband (zero output, otherwise); (iii) given $SOC_{l2} \le SOC_o < SOC_{h2}$, the BESS output is driven by the reference curve, i.e., $(L + H)/2$; (iv) given $SOC_{l1} \le SOC_o < SOC_{l2}$, the BESS output follows L outside the deadband (zero output, otherwise); and (v) given $SOC_o < SOC_{l1}$, the BESS only charges at a negative L. This strategy ensures that the SOC can be maintained within or recovered to an "optimal"

region (i.e., $SOC_{l2} \le SOC < SOC_{h2}$). Furthermore, for the "acceptable" regions of $SOC_{h2} \le SOC < SOC_{h1}$ and $SOC_{l1} \le SOC < SOC_{l2}$, the BESS output is set to 0 when the frequency locates within the deadband. This can reduce the cycles of the BESS and avoid the cost of energy used inside the deadband which would otherwise be incurred by the EFR asset.

In the eventuality that the BESS is close to an empty (or full) state, the required EFR output might not be possible, i.e., drawing more energy than available (or charging the BESS over the maximum limit). For this reason, discharge and charge rates of the BESS (denoted by P_{BESS}^{dis} and P_{BESS}^{ch}) are limited by Equations (1) and (2), respectively:

$$P_{BESS}^{dis} \le \frac{RC \cdot (SOC_o - SOC_{min})}{\Delta t / \eta_{dis}}, \quad (1)$$

$$\left| P_{BESS}^{ch} \right| \le \frac{RC \cdot (SOC_{max} - SOC_o)}{\Delta t \cdot \eta_{ch}}, \quad (2)$$

where Δt is the time step length used by the simulation; SOC_{min} and SOC_{max} denote the minimum and maximum permissible SOC levels; η_{dis} and η_{ch} are the efficiencies of discharging and charging, respectively; and RC is the remaining capacity reflecting the degradation of BESS energy capacity.

One of the most common charging methods, constant current-constant voltage (CC-CV) which adopts a high C-rate current [23], is used here to additionally limit the charge rate of the Lithium-Ion BESS. In a CC-CV charging profile, the BESS is charged at a constant current until the maximum allowable battery voltage is reached; then the charge rate exponentially decreases with time so as to maintain a constant battery voltage at the maximum acceptable level [24]. Since the output of the BESS for the EFR provision is driven by the frequency deviation from 50 Hz, the charge phase may be not continuous in time. Therefore, the charging profile which correlates the maximum allowable charge rate with the time cannot be directly applied in this study. It is found that the time-dependent limit on $\left| P_{BESS}^{ch} \right|$ can be converted into the SOC-dependent limit which equals the rated power P_{BESS}^{rated} before the SOC reaches the level (e.g., 80% [24]) at which the CC stage terminates and then linearly decreases to a pre-determined cut-off level (e.g., 5% of P_{BESS}^{rated}) until the BESS is fully charged.

Based on the BESS output determined from the EFR envelopes subject to the SOC-related constraints, the SOC is updated via Equation (3), and wind power is curtailed via Equation (4) whenever the ampacity of the connection point (P_{CON}) is reached as to allow the BESS to deliver the determined EFR (P_{EFR}^{NPE}):

$$SOC_{new}^{NPE} = \begin{cases} SOC_o - (P_{EFR}^{NPE} \cdot \Delta t)/(\eta_{dis} \cdot RC), & for\ P_{EFR}^{NPE} > 0 \\ SOC_o - (P_{EFR}^{NPE} \cdot \Delta t \cdot \eta_{ch})/RC, & for\ P_{EFR}^{NPE} < 0 \end{cases}, \quad (3)$$

$$P_{WF}^{sell} = min(P_{WF}^{tot}, P_{CON} - P_{EFR}^{NPE}), \quad (4)$$

where the wind power (P_{WF}^{sell}) flowing to the connection point via WFm is the minimum of available wind power (P_{WF}^{tot}) or the remaining ampacity of the connection point. In addition to updating the SOC based on the BESS export/import, an accurate real-time SOC monitoring is required in practice to follow the coordination strategy and meet the SOC-related operational requirement. For the methods available to the practical SOC monitoring, the reader is referred to [25] which has detailed the SOC estimation methods.

2.3.2. ENPE Coordination Strategy

The ENPE strategy determines a temporary EFR delivery in the same way as the NPE does, i.e., $P_{EFR}^{tem} = P_{EFR}^{NPE}$. Then, the ENPE strategy reduces P_{EFR}^{tem} within the EFR envelopes to accommodate the wind generation which would otherwise be curtailed. The decrease from P_{EFR}^{tem} to an adjusted EFR (i.e., P_{EFR}^{ENPE}) driven by the wind curtailment is permitted only when P_{EFR}^{tem} is within EFR envelopes and the SOC after the delivery of P_{EFR}^{tem} (i.e., SOC_t^{tem}) would be smaller than a particular SOC-related strategy variable (i.e., SOC_r):

$$P_{EFR}^{ENPE} = \begin{cases} max(L, P_{CON} - P_{WF}^{tot}), & for\ P_{WF}^{tot} + P_{EFR}^{tem} > P_{CON} \cap SOC_t^{tem} < SOC_r \cap L < P_{EFR}^{tem} \le H \\ P_{EFR}^{tem}, & otherwise \end{cases} \quad (5)$$

Then, the SOC-related operational limits are used again to constraint P_{EFR}^{ENPE}. Finally, the SOC of the BESS and the wind power transferred to WFm are updated using Equations (3) and (4) based on P_{EFR}^{ENPE}.

2.3.3. PE Coordination Strategy

The PE strategy uses an additional converter (AdC) to exchange power between the BESS and the WF (see Figure 2b). The BESS can capture the wind generation that would otherwise be curtailed due to the limited power capacity of the connection point and transfer the surplus energy to WFm which is then sold as wind energy. Two additional SOC-related strategy variables (i.e., $SOC_{ld} \le SOC_{hc}$) are specified in this strategy to control the power exchange between WF and BESS.

The EFR delivery and P_{WF}^{sell} are first determined in the same way as in the ENPE (i.e., $P_{EFR}^{PE} = P_{EFR}^{ENPE}$) which is then used to estimate the SOC after the P_{EFR}^{PE} delivery (i.e., SOC_t^{PE}). If SOC_t^{PE} is above SOC_{ld}, the surplus energy of BESS is allowed to transfer to WFm and sold as wind energy (i.e., P_{BESS}^{sell}) subject to the available ampacity of connection point, the power rating of the AdC (i.e., P_{AdC}^{r}), and the remaining power capacity of the BESS:

$$P_{BESS}^{sell} = \begin{cases} min\left[\frac{(SOC_t^{PE} - SOC_{ld}) \cdot RC}{\Delta t / \eta_{AdC}^{D2A}}, (P_{CON} - P_{WF}^{sell} - P_{EFR}^{PE}), P_{AdC}^{r}, \mathbb{B}^{+}(P_{BESS}^{rated}, P_{EFR}^{PE})\right], & for\ SOC_t^{PE} > SOC_{ld} \\ 0, & otherwise \end{cases} \quad (6)$$

where the term η_{AdC}^{D2A} is the efficiency of the AdC inverting DC to AC. The operator $\mathbb{B}^{+}(\cdot)$ determines the maximum allowable discharge rate through the AdC given the BESS delivering P_{EFR}^{PE} at the same moment:

$$\mathbb{B}^{+}(P_{BESS}^{rated}, P_{EFR}^{PE}) = \begin{cases} (P_{BESS}^{rated}/\eta_{dis} - P_{EFR}^{PE}/\eta_{dis}) \cdot \eta_{AdC}^{D2A}, & for\ P_{EFR}^{PE} \ge 0 \\ (P_{BESS}^{rated}/\eta_{dis} - \eta_{ch} \cdot P_{EFR}^{PE}) \cdot \eta_{AdC}^{D2A}, & for\ P_{EFR}^{PE} < 0 \end{cases} \quad (7)$$

If SOC_t^{PE} is lower than SOC_{hc}, the BESS is operated to store the otherwise curtailed wind power (i.e., P_{WF}^{store}) subject to P_{AdC}^{r} and the remaining power capacity of the BESS:

$$P_{WF}^{store} = \begin{cases} min\left[\frac{(SOC_{hc} - SOC_t^{PE}) \cdot RC}{\Delta t \cdot \eta_{AdC}^{A2D}}, (P_{WF}^{tot} - P_{WF}^{sell}), P_{add}^{r}, \mathbb{B}^{-}\left(\left|\underline{P}_{BESS}^{ch}(SOC_o)\right|, P_{EFR}^{PE}\right)\right], for\ SOC_t^{PE} < SOC_{hc}, \\ 0, \quad otherwise \end{cases} \quad (8)$$

where η_{add}^{A2D} denotes the efficiency of the AdC rectifying AC to DC. The operator $\mathbb{B}^{-}(\cdot)$ calculates the magnitude of maximum allowable charge rate through the AdC given the BESS delivering P_{EFR}^{PE} at the same moment:

$$\mathbb{B}^{-}\left(\left|\underline{P}_{BESS}^{ch}(SOC_o)\right|, P_{EFR}^{PE}\right) = \begin{cases} \left(\eta_{ch} \cdot \left|\underline{P}_{BESS}^{ch}(SOC_o)\right| + P_{EFR}^{PE}/\eta_{dis}\right)/\eta_{AdC}^{A2D}, & for\ P_{EFR}^{PE} \ge 0 \\ \left(\eta_{ch} \cdot \left|\underline{P}_{BESS}^{ch}(SOC_o)\right| + \eta_{ch} \cdot P_{EFR}^{PE}\right)/\eta_{AdC}^{A2D}, & for\ P_{EFR}^{PE} < 0 \end{cases} \quad (9)$$

where $\left|\underline{P}_{BESS}^{ch}(SOC_o)\right|$ denotes the magnitude of the SOC-dependent maximum allowable charge rate derived from the CC-CV charging profile. Then, the total power transferred to WFm is calculated as $(P_{WF}^{sell} + P_{BESS}^{sell})$ and the SOC of the BESS is updated using:

$$SOC_{new}^{PE} = \begin{cases} SOC_o - (P_{EFR}^{PE}/\eta_{dis} + P_{BESS}^{sell}/\eta_{AdC}^{D2A} - P_{WF}^{store} \cdot \eta_{AdC}^{A2D}) \cdot \Delta t/RC, & for\ P_{EFR}^{PE} \ge 0 \\ SOC_o - (P_{EFR}^{PE} \cdot \eta_{ch} + P_{BESS}^{sell}/\eta_{AdC}^{D2A} - P_{WF}^{store} \cdot \eta_{AdC}^{A2D}) \cdot \Delta t/RC, & for\ P_{EFR}^{PE} < 0 \end{cases} \quad (10)$$

where the discharge and charge efficiencies of the two converters are assumed to be 0.95 in this study.

Compared with the control strategies designed by Greenwood et al. [4], Gundogdu et al. [5], and Canevese et al. [26] which aimed to maintain the SOC of a stand-alone BESS within a single target range while providing EFR services, the paper additionally specify-

ing the critical regions, i.e., $SOC_o \geq SOC_{h1}$ or $SOC_o \leq SOC_{l1}$ where the BESS is only permitted to export or import, respectively, is expected to mitigate the excessive charge or discharge that accelerates the battery degradation. Furthermore, the ENPE or PE strategy developed here takes into account available power outputs of the co-located WF and introduces additional SOC-related strategy variables to alleviate wind curtailment caused by the limited ampacity of their common connection point. Compared with the control methods of WF + BESS systems designed by Munoz-Vaca et al. [21] and Johnston et al. [27] where the BESS assisted the WF in the FR delivery and permitted the WF to generate close to available power outputs, the paper focuses on a direct use of the co-located BESS for the EFR service provision via the existing connection point of the WF. In addition, optimisation results of these SOC-related strategy variables that maximise the net profit of the co-located system will indicate the optimal coordination between WF and BESS under a particular control strategy.

2.4. Modelling of Lithium-Ion Battery Degradation

Since the cost of the BESS is substantial, it is necessary to model the battery degradation which will greatly affect the economic viability. The degradation of a Lithium-Ion battery is influenced by several factors such as cell temperature, SOC, depth of discharge (DOD), etc. Presuming that a Lithium-Ion battery could withstand a particular volume of cumulative charge flow before the end-of-life given certain C-rate and average cell temperature, an energy-throughput model was used by Wu et al. [28,29] to estimate the energy capacity loss associated with the cycle ageing in each simulation time step. In this work, the degradation of a Lithium-Ion battery $f_d(\cdot)$ over a particular time period td is modelled as a combination of the calendar ageing $f_t(\cdot)$ and the cycle ageing $f_c(\cdot)$ that are linearly related to the number of cycles [30]:

$$f_d\left(td, \varepsilon_i, \sigma_i, T_{c,i}\right) = f_t(td, \bar{\sigma}, \bar{T}_c) + \sum_{i=1}^{N_c} f_c\left(\varepsilon_i, \sigma_i, T_{c,i}\right) \tag{11}$$

where terms ε_i, σ_i, and $T_{c,i}$ represent DOD, average SOC, and average cell temperature of the i^{th} cycle ($i = 1, \ldots, N_c$) over td respectively; $\bar{\sigma}$ and $\bar{T}_c$ are averages of σ_i and $T_{c,i}$ over td respectively.

Standard battery tests are usually performed cycling at constant DOD. Considering that in this study the DOD is not constant, the rainflow counting algorithm [31] is used to divide the time series of SOC over td into individual partial charge/discharge cycles on which the degradation is computed. The daily degradation of the BESS (i.e., $td = 24\ hr$) is modelled here assuming a constant $T_{c,i}$ of 20 ℃. The remaining energy capacity at the end of D days (denoted by RC_D) is updated based on the sum of the daily degradation $f_{d,j}$, $j = 1, \ldots, D$:

$$RC_D = C_{BESS}^{rated} \cdot \left[1 - \alpha_{SEI} e^{-\beta_{SEI} \sum_{j=1}^{D} f_{d,j}} - (1 - \alpha_{SEI}) e^{-\sum_{j=1}^{D} f_{d,j}}\right] \tag{12}$$

where C_{BESS}^{rated} denotes the energy rating of the BESS; α_{SEI} and β_{SEI} are coefficients for the solid electrolyte interphase (SEI) model which includes the life-dependence characteristic of the battery degradation [30]. The parameters of the degradation model tuned in [30] for a Lithium-Ion LMO battery are adopted here to update the remaining energy capacity at the end of each day.

3. Particle Swarm Optimisation-Based Sizing Algorithm

3.1. Revenue and Cost of Consolidating BESS in the UK

3.1.1. Revenue of EFR Service

The revenue of the EFR provision depends on the service performance measure (SPM) over each half-hour settlement period (SP) which is calculated as the average of second by second performance measure (SBSPM) over that SP. If the response delivery is within the

EFR envelopes (e.g., $L \le P_{EFR}^{PE} \le H$) at a particular second, the SBSPM is set to 1; otherwise, the SBSPM is estimated from the deviation between P_{EFR}^{PE} and the envelopes with the following:

$$SBSPM = \begin{cases} 1 - (P_{EFR}^{PE} - H)/P_{EFR}^{cap}, & for\ P_{EFR}^{PE} > H \\ 1 - (L - P_{EFR}^{PE})/P_{EFR}^{cap}, & for\ P_{EFR}^{PE} < L \\ 1, & otherwise \end{cases} \quad (13)$$

The SPM calculated from the SBSPM within the SP is used to generate an availability factor (AF), as tabulated in Table 1. Given the tendered price $\mathcal{P}_{EFR}$ (which here is considered to be the average price of the first EFR tender and equal to GBP 9.44/MW of EFR/hr [11]), the EFR payment in a SP (i.e., $R_{EFR,sp}^{AF}$) is calculated by:

$$R_{EFR,sp}^{AF} = P_{EFR}^{cap} \cdot \mathcal{P}_{EFR} \cdot AF \cdot 0.5hr \quad (14)$$

Table 1. Conversion from service performance measure (SPM) to available factor (AF)

SPM	0% ~ 50%	50% ~ 75%	75% ~ 95%	95% ~ 100%
AF	0%	50%	75%	100%

As was noted in Section 2.3.1, an EFR provider is responsible for any costs of energy imbalances whilst inside the deadband [32]. The energy imbalance may be bought from or sold to the system based on the System Buy Price (SBP) and System Sell Price (SSP) which reflect the cost of balancing the transmission system for a particular SP [33]. A single price calculation is currently applied such that SSP and SBP are the same in each SP [33]. The revenue/cost related to the energy imbalance (i.e., $R_{EFR,sp}^{IMB}$) inside the deadband over a SP is estimated by:

$$R_{EFR,sp}^{IMB} = \bar{P}_{EFR}^{ins} \cdot \mathcal{P}_{IMB} \cdot 0.5hr \quad (15)$$

where $\bar{P}_{EFR}^{ins}$ (MW) and $\mathcal{P}_{IMB}$ (GBP/MWh) are the average EFR delivery inside the deadband and the imbalance price (i.e., SSP/SBP) in the SP, respectively.

3.1.2. Monetary Gain or Loss Related to Wind Generation (WG)

As was noted in Section 2.3, the EFR delivery by the co-located BESS may lead to the curtailment of WG due to the limited ampacity of their common connection point, while the converter between WF and BESS could enable the time shift of WG and put the otherwise curtailed WG onto the grid. The differences in the power passing through WFm (denoted by δP_{WF}^{sell}) between the wind + BESS system and a single WF without a BESS mean monetary gains or losses related to WG. Given the output of a single WF being the minimum of P_{WF}^{tot} or P_{CON}, δP_{WF}^{sell} due to the co-location of a BESS along with the use of, e.g., PE strategy is calculated by:

$$\delta P_{WF}^{sell} = P_{WF}^{sell} + P_{BESS}^{sell} - min(P_{WF}^{tot}, P_{CON}) \quad (16)$$

The WG-related monetary gain/loss in a SP (i.e., $\delta R_{WG,sp}$) is then estimated based on δP_{WF}^{sell} taking imbalance prices and ROC [14] into account:

$$\delta R_{WG,sp} = \delta \bar{P}_{WF}^{sell} \cdot (\mathcal{P}_{IMB} + \mathcal{P}_{ROC}) \cdot 0.5hr \quad (17)$$

where $\delta \bar{P}_{WF}^{sell}$ is the average of δP_{WF}^{sell} in the SP and $\mathcal{P}_{ROC}$ denotes the price at which the WF sells the ROCs issued for every MWh of its accredited generation to electricity suppliers. Presuming that 2 ROCs would be issued to a particular offshore WF for each MWh of its generation [14], $\mathcal{P}_{ROC}$ is approximated here to be GBP 50.05/ROC of 2 ROCs/MWh, i.e., GBP 100.1/MWh based on the buy-out price of GBP 50.05/ROC for 2020/2021 [34]. A positive $\delta \bar{P}_{WF}^{sell}$ means that the WF consolidated with a BESS will be paid more than a single WF by an amount of $\delta R_{WG,sp}$ in the SP, and vice versa. Considering that ROCs will be issued until the year 2037 and that the anticipated difference between average strike price and average reference price paid to the CFD offshore WG, i.e., (GBP 160.28/MWh—GBP

55.15/MWh) = GBP 105.13/MWh [35], is close to $\mathcal{P}_{ROC}$ adopted here, the paper simulates the renewable energy subsidy under the RO scheme only.

3.1.3. CAPEX and OPEX of Lithium-Ion BESS and Connection

The capital expenditure (CAPEX) of a Lithium-Ion BESS mainly comprises the costs of battery, converter, and balance-of-system (BOS) [36]. The price trend of Lithium-Ion battery modelled by Campos-Gaona et al. [7] based on high-profile reports is used here to estimate the battery price in the year 2020, i.e., GBP 128/kWh. The price of the converter for utility-scale BESS and the BOS are assumed here to be GBP 66/kW and 30% of the total cost of Lithium-Ion battery and converter, respectively [36]. Then, the CAPEX of a Lithium-Ion BESS with P_{BESS}^{rated} and C_{BESS}^{rated} is calculated by GBP $130\% \cdot (128k \cdot C_{BESS}^{rated} + 66k \cdot P_{BESS}^{rated})$. It is noted that the use of the additional converter with P_{AdC}^{r} increases the CAPEX by GBP $130\% \cdot 66k \cdot P_{AdC}^{r}$.

The annual operational expenditure (OPEX) of a Lithium-Ion BESS excluding the electricity cost is assumed here to be 2% of its CAPEX [36]. In addition to CAPEX and OPEX of the BESS itself, co-locating the BESS to a transmission-connected WF in the GB incurs a number of connection charges:

1. Application fee:
   Prior to grouping the BESS within an existing connection site, a modification application is required to review and potentially amend the existing connection agreement [37]. The application fee depending on the connection zone and the change of transmission entry capacity (TEC) is calculated using an application fee calculator [38] provided by the NGESO. It is noted that a new, independent connection of a stand-alone BESS to the transmission system requires a new application [37] which differs from the modification application in the cost [38].
2. Transmission Network Use of System (TNUoS) charge:
   Generators using the GB transmission networks to deliver electricity need to pay TNUoS charges to the NGESO [39] which largely depend on the type of the generator. A stand-alone BESS is charged as a conventional carbon generator while a wind + BESS system (i.e., a combination of intermittent and conventional carbon) would be charged according to its predominant fuel type under the present charging methodologies [39]. In the case of the predominant fuel type being intermittent, the increase of annual TNUoS charge (denoted by $\delta TNUoS$) due to the co-located BESS depends on the growth of annual load factor (ALF). Since an ALF of around 10.8% would be used for a BESS prior to any historic data being available [32], the ALF of the wind+BESS system is presumed to increase by $(10.8\% \cdot P_{BESS}^{rated}/P_{CON})$ in this study where the consolidation does not change the TEC.
3. Balancing Services Use of System (BSUoS) charge:
   BSUoS charges paid by generators and suppliers recover the costs of balancing services activities undertaken by the NGESO including the operation of transmission system and the balancing services procured and used to balance the transmission system [40]. Based on the BSUoS price (GBP/MWh) [40] in a SP, the change of the BSUoS charge (i.e., $\delta BSUoS_{sp}$) after the co-location of the BESS is computed from the difference in the net electricity passing through the connection point in the SP which equals $(\delta \bar{P}_{WF}^{sell} + \bar{P}_{EFR}^{PE}) \cdot 0.5hr$ where $\bar{P}_{EFR}^{PE}$ is the average EFR delivery over the SP.

According to the characteristics of the connection charges above, the application fee is regarded as the CAPEX of the connection, and changes of TNUoS and BSUoS charges are regarded as the OPEX of the connection. It is noted that the charges for new assets or reinforcements (NAoR) required to connect a stand-alone BESS would additionally contribute to CAPEX and OPEX of its independent connection. Table 2 compares components in CAPEX and OPEX between independent and co-located connections.

Table 2. CAPEX (GBP) and OPEX (GBP) of independently connecting a stand-alone BESS or co-locating a BESS with an existing wind farm without changing the TEC.

Connection Type		Independent	Co-Located w/o TEC Change
CAPEX (GBP)	Application fee [1]	$34{,}860 + 226.2 \times P_{BESS}^{rated}$	26,145
	NAoR capital cost [2]	6,240,000	N/A
OPEX (GBP)	δTNUoS [3]	$715.86 \times P_{BESS}^{rated}$ per yr.	$919.573 \times P_{BESS}^{rated}$ per yr.
	$\delta BSUoS_{sp}$	$\bar{P}_{EFR}^{PE}$ related	$(\delta\bar{P}_{WF}^{sell} + \bar{P}_{EFR}^{PE})$ related
	NAoR non-capital cost [2]	147,538 per yr.	N/A

[1] based on the medians of bases and rates in different connection zones [38];.[2] for a new connection of ≤90 MW to a 132 kV, 0.5 km-away substation in rural area [41];[3] based on an ALF of 10.8% for BESS and TNUoS tariffs for the 9th generation zone in 2019/20 [42].

3.2. Particle Swarm Optimisation-Based Sizing Algorithm

Based on the simulation model of the wind + BESS system outlined in Section 2 combined with revenues and costs of the co-located system described in Section 3.1, the optimisation variables in each coordination strategy including the BESS size and SOC-related strategy variables are estimated to maximise the net present value (NPV) [43] of the project at the end of a 4-year EFR contract:

$$\max\left\{-CAPEX_{BESS} - CAPEX_{CON} + \sum_{m=1}^{48} \frac{R_{EFR,m}^{AF} + R_{EFR,m}^{IMB} + \delta R_{WG,m} - \delta TNUoS_m - \delta BSUoS_m - OPEX_{BESS,m}}{(1+d)^{m/12}}\right\} \quad (18)$$

subject to:

$$0MW \le P_{AdC}^{r} \le 50MW \quad (19)$$

$$1MW \le P_{BESS}^{rated} \le 50MW \quad (20)$$

$$C_{BESS}^{rated} - P_{BESS}^{rated} \cdot 0.25/\eta_{dis} \ge 0 \quad (21)$$

$$ASPM_n \ge 0.95,\ \ n = 8760 \cdot 2, \ldots, (8760 \times 4 + 24) \times 2 \quad (22)$$

$$SOC_{l1} < SOC_{ld} < SOC_{hc} < SOC_{h1} \quad (23)$$

$$RC_{end} \ge 80\% \cdot C_{BESS}^{rated} \quad (24)$$

where $CAPEX_{BESS}$ and $CAPEX_{CON}$ are the one-off CAPEX of the BESS and its connection. Given that most of the other revenues and costs included in this study are monthly billed, present values of the monthly EFR payment $R_{EFR,m}^{AF}$, EFR imbalance related revenue/cost $R_{EFR,m}^{IMB}$, WG-related monetary gain/loss $\delta R_{WG,m}$, TNUoS charge change $\delta TNUoS_m$, BSUoS charge change $\delta BSUoS_m$, and OPEX of the BESS $OPEX_{BESS,m}$ over the m^{th} $(m = 1, \ldots, 48)$ month are discounted using an annual return $d = 8\%$. Furthermore, the constraints specified by Equations (20)—(22) fulfil the technical requirement of the EFR service [22]: (i) the contracted EFR capacity P_{EFR}^{cap} reflected by P_{BESS}^{rated} (i.e., $P_{EFR}^{cap} = P_{BESS}^{rated}$) is between the minimum and maximum contract capacities; (ii) the BESS provider has the capability of delivering at 100% of P_{BESS}^{rated} for at least 15 min; and (iii) the average of all SPMs over a rolling 12-month period (i.e., $ASPM_n$) calculated at the end of each half-hour SP should be greater than or equal to 95%. The limits specified in Equations (23) for the PE strategy mitigate the impact of the time shift of WG on the performance of EFR delivery. In addition, Eq. (24) formulates a specific requirement that the final remaining energy capacity of the BESS (i.e., RC_{end}) at the end of the 4-years should be at least 80% of C_{BESS}^{rated}.

The calculation of the optimisation variables from Equations (18)—(24) is implemented by the particle swarm optimisation (PSO) algorithm [44,45] that minimises an objective function starting from a set of randomly generated particles which travel in the

problem space until convergence is reached. The PSO has a range of key advantages in resolving the non-smooth global optimisation problems, e.g., derivative-free, high-quality solutions within less computation time and more stable convergence than other stochastic methods [46].

The ideas are demonstrated here based on 1-min average outputs of a particular 76 MW WF (the data source is undisclosed due to confidentiality) with an estimated connection size of 68.4 MW (i.e., 90% of its installed capacity [47]), BSUoS prices [40], imbalance prices [48], and 1-sec grid frequencies [49] in the GB over 4 years from 2015 to 2018.

4. Results and Model Validation

All simulation models and mathematical calculations in the work presented here are undertaken using MATLAB/Simulink [50]. Four scenarios are investigated in this section including (i) a stand-alone BESS using NPE strategy and wind + BESS systems using (ii) NPE strategy, (iii) ENPE strategy, and (iv) PE strategy. The PSO-based simulation results and the revenues and costs of different scenarios will be assessed, showing the effectiveness of the BESS sizing algorithm and the profits of co-locating a BESS with a WF for the stacking of multiple revenue streams.

4.1. Assessment of PSO Based Simulation Results

Table 3 lists the optimisation variables in each scenario determined by the PSO algorithm where the convergence of optimisation variables and final NPV in, e.g., scenario (iii) is plotted in Figures 3 and 4, respectively. In all the scenarios, the optimised C_{BESS}^{rated} equals the minimum required by the EFR regulations (i.e., the BESS needs to be able to deliver P_{BESS}^{rated} for a minimum of 15 min); and P_{BESS}^{rated} equalling the maximum contract EFR capacity means that the increase of the EFR payment with P_{BESS}^{rated} is higher than the total growth of CAPEX and OPEX of the BESS and its connection. It is noted that the ordinary PSO algorithm employed here to deal with multivariable optimisation may fall in the local optimum or premature solution [51]. In practice however in our case, given a large number of randomly initialised particles, the algorithm converges always to the same solution between different runs, suggesting that the global minima could have been found in the search area. Though the optimised BESS capacity along with SOC-related strategy variables in Table 3 are considered to provide a reasonable trade-off between revenue and investment of the co-located system based on the following operational and economic analysis, the optimisation algorithm for the BESS sizing could be enhanced to permit a global optimum solution [51].

Table 3. Optimisation variables determined by the PSO algorithm in each scenario.

Scenario	Optimised Variables									
	P_{BESS}^{rated} (MW)	C_{BESS}^{rated} (MWh)	P_{AdC}^{r} (MW)	SOC_{l1} (%)	SOC_{l2} (%)	SOC_{h2} (%)	SOC_{h1} (%)	SOC_{r} (%)	SOC_{ld} (%)	SOC_{hc} (%)
(i)	50	13.16	n/a	0.11	39.65	40.10	99.29	n/a	n/a	n/a
(ii)	50	13.16	n/a	0.08	34.26	34.26	34.26	n/a	n/a	n/a
(iii)	50	13.16	n/a	0	5.52	5.91	99.57	98.91	n/a	n/a
(iv)	50	13.16	7	0	97.81	97.81	97.81	73.16	19.56	33.13

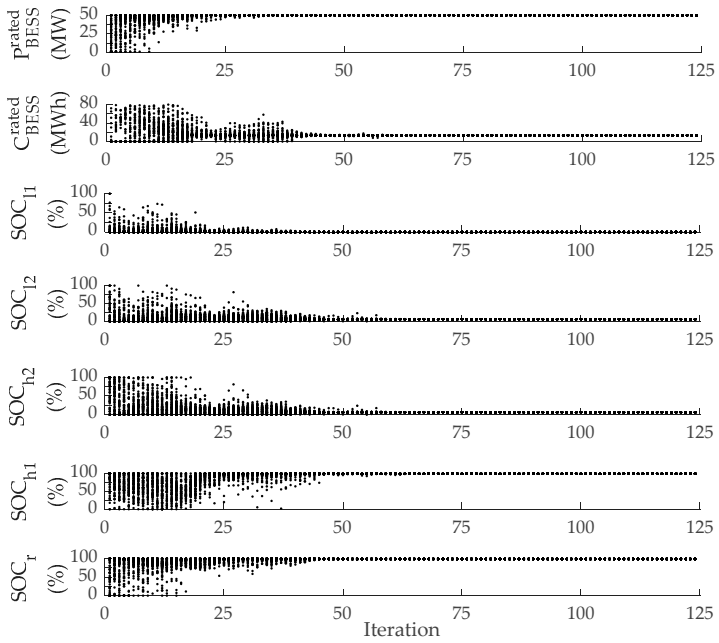

Figure 3. Convergence of optimisation variables in the PSO algorithm for scenario (iii).

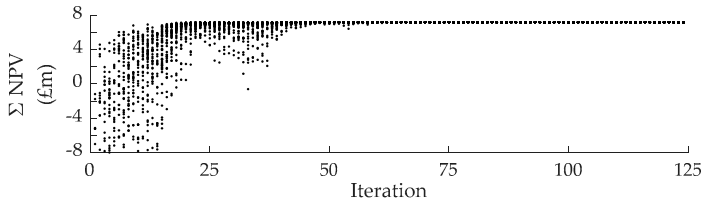

Figure 4. Convergence of final NPV in the PSO algorithm for scenario (iii).

Based on the optimisation variables determined in scenario (iii), the BESS operation driven by the frequency deviation under ENPE strategy is simulated for 4 years. The SOC fluctuation and the resulting battery degradation are shown in Figure 5 where RC_{end} is greater than 80% of C^{rated}_{BESS}. Data pairs of BESS outputs (+ ve for discharge rate and − ve for charge rate) against the SOC are plotted in Figure 6 where magnitudes of charge rates are well maintained below the SOC-dependent limits. Furthermore, the ASPM over a rolling 12-month period simulated in each scenario is greater than 99.9%, 98.3%, 99.3%, and 99.8%, respectively which are all above the minimum requirement of 95%.

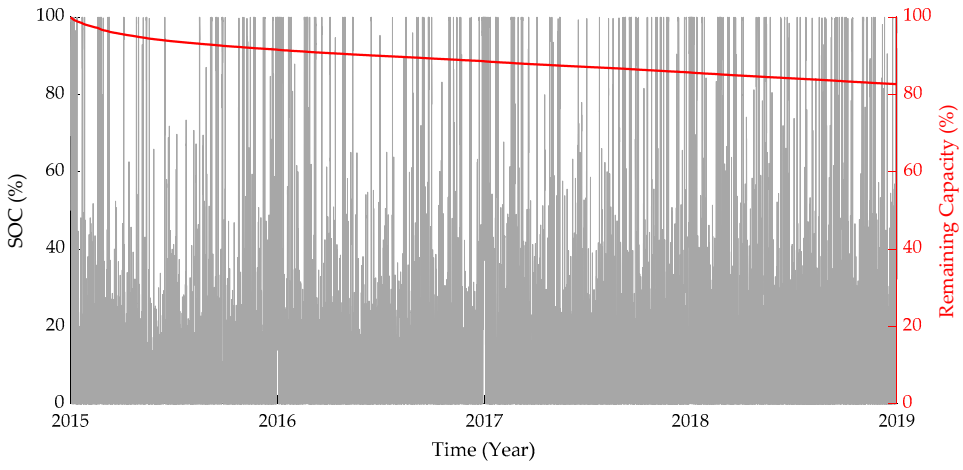

Figure 5. The SOC and remaining capacity of the BESS simulated over 4 years in scenario (iii).

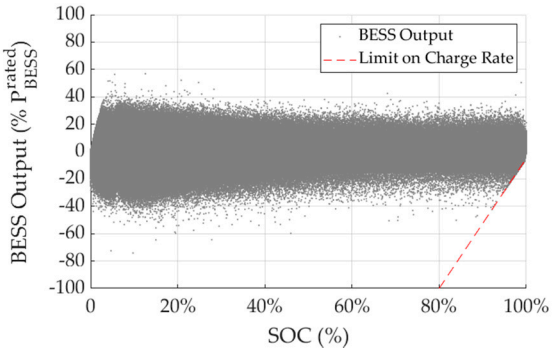

Figure 6. Data pairs of the discharge (+ve)/charge (−ve) rate against SOC simulated in scenario (iii).

4.2. EFR Performance and BESS Usage

Each scenario is simulated for 4 years using the PSO-based optimisation variables in Table 3. For the four scenarios, the distribution of the SPM within the ranges defined in Table 1 is shown in Figure 7, while Figure 8 shows the SOC frequency distribution. The SPM values are shown to exceed 95% for at least 90% of the time in each scenario. Furthermore, the SOC of the BESS is shown to remain at a low level for most of the time since the modelled battery degradation reduces with a relatively lower SOC [30].

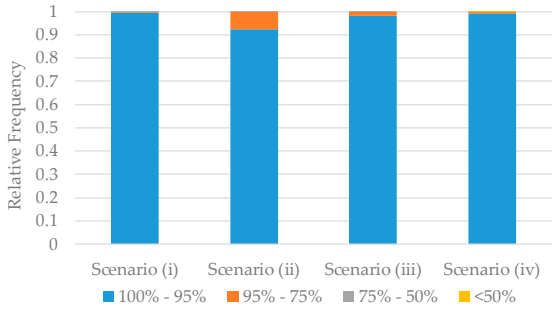

Figure 7. SPM distributions relative to the ranges defined in Table 1 in the four scenarios.

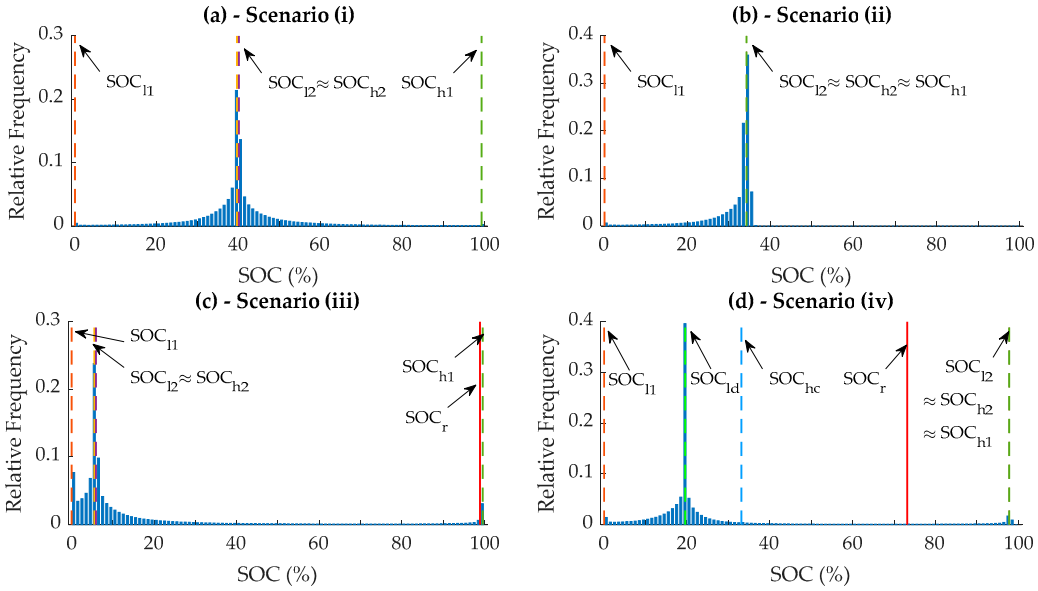

Figure 8. Frequency distributions of the SOC of the BESS in the four scenarios. (**a**) Scenario (i); (**b**) Scenario (ii); (**c**) Scenario (iii); (**d**) Scenario (iv).

Since the EFR payment is the only revenue stream to be maximised in Scenario (i), the four SOC-related strategy variables are optimised such that the stand-alone BESS can have sufficient energy or space to deliver the EFR volume as required. Figure 8a shows that the BESS operates around SOC_{l2} and SOC_{h2} of about 40% for most of the time. Operating within this SOC range allows the BESS to respond to different frequency events. Figure 7 shows that the BESS in Scenario (i) provides a better EFR performance in terms of SPM than the other scenarios where there is a trade-off between EFR- and wind generation (WG)-related revenues.

In Scenario (ii), the optimised values of SOC_{l2}, SOC_{h2} and SOC_{h1} are almost the same. Since the BESS is designed to export only when its SOC exceeds SOC_{h1}, Figure 8b shows that the BESS operates within the lower 'acceptable' region (i.e., SOC_{l1}~SOC_{l2}) for around 70% of the time where the EFR delivery follows the lower envelope outside the deadband. This helps alleviate the WG curtailment which in turns results in occasional under-delivery of EFR, leading to the reduction of EFR-related revenues (the SPM is smaller than 95% for more than 7% of the time, as shown in Figure 7).

Compared to the NPE strategy adopted in Scenario (ii), the ENPE strategy used in Scenario (iii) can adjust the EFR delivery within the envelopes if the SOC is less than SOC_r of 98.91% in order to enable additional WG which would otherwise be curtailed due to the limited ampacity of the connection point. Figure 9 shows a particular case occurred at 01:44:00 on 03/01/2015 where the temporary EFR delivery (i.e., P_{EFR}^{tem}) of the BESS with SOC of 46.64% would follow the upper envelope of 13.78 MW, leading to a WG curtailment of about 2.38 MW. In this occasion, the ENPE strategy decreased the delivery of EFR from 13.78 MW to 11.4 MW, which provided 2.38 MW headroom in the ampacity of the connection point for exporting the otherwise curtailed WG. Therefore, the BESS under the ENPE strategy in Scenario (iii) is able to accommodate WG while providing a better EFR performance than the BESS under the NPE strategy in Scenario (ii), as shown in Figure 7.

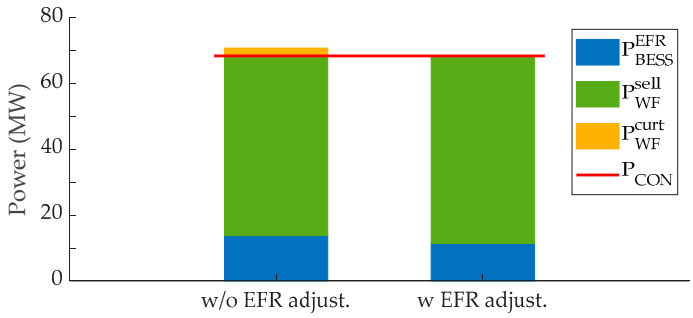

Figure 9. EFR delivery decreasing from the upper envelope of 13.78 MW to an appropriate level of 11.4 MW to avoid 2.38 MW WG curtailment at 01:44:00 on 03/01/2015 under the ENPE strategy.

In Scenario (iv), SOC_{l2}, SOC_{h2} and SOC_{h1} are optimised to have the same value of 97.81%. The BESS mostly operates within the lower acceptable region where the EFR delivery adheres to the lower envelope outside the deadband while the response following the reference curve inside the deadband can be adjusted to alleviate WG curtailment if the SOC is smaller than SOC_r of 73.16%. Furthermore, the 7 MW additional converter (AdC) placed between BESS and WF enables their power exchange. For example, 6.92 MW of 12.84 MW WG curtailment was injected into the BESS via the 7 MW AdC at 02:21:00 on 04/01/2015, as shown in Figure 10a, which increased the SOC of BESS to SOC_{hc} of 33.13%. When the SOC of BESS exceeds SOC_{ld} of 19.56%, the surplus energy of BESS is transferred to WFm via the 7 MW AdC subject to the remaining ampacity of the connection point. Figure 10b gives an example where, in addition to the EFR delivery of 4.57 MW at 03:03:00 on 04/01/2015, the BESS discharged 7 MW to WFm with its SOC reducing from 33.13% to 31.62%. Moreover, Figure 8d shows that the SOC concentrates around SOC_{ld}, which means that the BESS mostly delivers its surplus energy to WFm given its SOC exceeding

SOC_{ld} so as to increase the WG-related revenue. In addition, operating around SOC_{ld} of 19.56% enables a satisfactory EFR performance as shown in Figure 7.

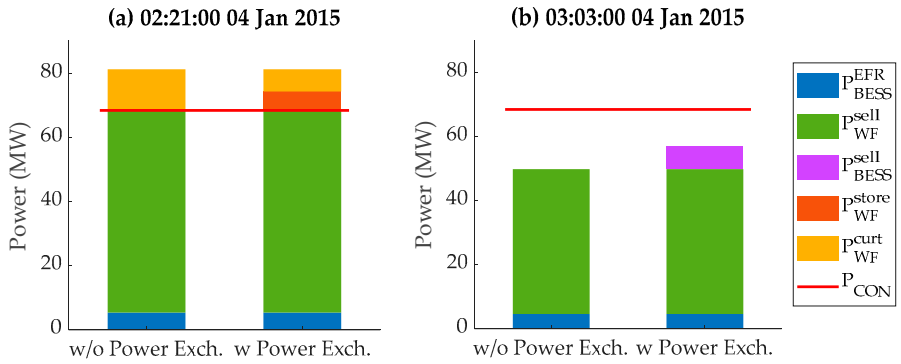

Figure 10. The BESS (**a**) stored 6.92 MW WG which would otherwise be curtailed at 02:21:00 and (**b**) delivered 7 MW to WFm at 03:03:00 on 4 January 2015 via the 7 MW AdC between BESS and WF.

4.3. Cost–benefit Analysis

It is noted that costs and revenues are referred to their present values in this section. Figure 11 compares cumulative cost and revenue components along with NPVs over 4 years in each scenario. Different scenarios are shown to obtain similar revenues by providing the EFR service while Scenario (iv) additionally achieves a significant WG-related revenue due to the power exchange between WF and BESS. Furthermore, the CAPEX of the BESS contributes to a significant part of the total cost. In addition, the independent connection of a stand-alone BESS to the transmission system in Scenario (i) could incur a significant charge for NAoR (i.e., contributing to CAPEX and OPEX of the connection), which largely reduces its final NPV.

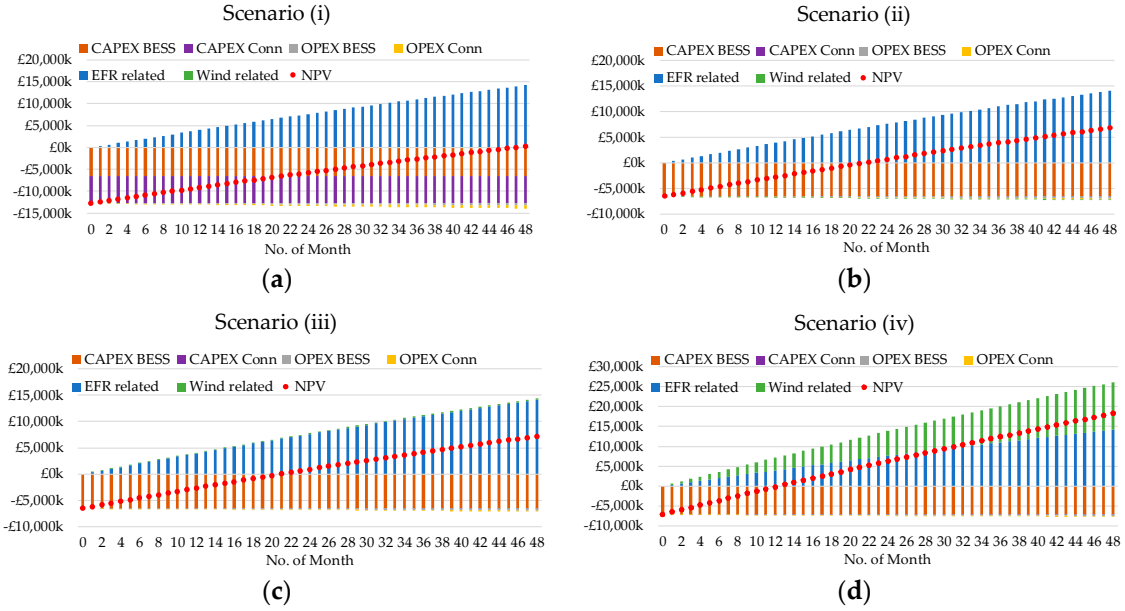

Figure 11. Cumulation of different cost and revenue components along with NPVs over 4 years in each scenario.

A breakdown of total costs and revenues at the end of the 4-years in each scenario is listed in Table 4. Although Scenario (iii) performs better in the EFR delivery than Scenario (ii) as shown in Figure 7, a smaller EFR-related revenue is achieved in Scenario (iii). This is because the response inside the deadband that coincides with WG curtailment is correspondingly reduced within the EFR envelopes under the ENPE strategy in Scenario (iii),

which decreases the value of R_{EFR}^{IMB}. However, the additional WG enabled in Scenario (iii) increases its WG-related revenue to GBP 278.7k which exceeds the reduction of the EFR-related revenue, leading to a higher final NPV than Scenario (ii). Furthermore, though the placement of the 7 MW AdC in Scenario (iv) increases the CAPEX and OPEX of BESS, it assists the BESS in the time shift of WG which significantly increases the WG-related revenue, leading to a much greater final NPV than the other three scenarios.

Table 4. A breakdown of total costs and revenues (thousand GBP) at the end of 4 years in each scenario.

Item		Scenario (i)	Scenario (ii)	Scenario (iii)	Scenario (iv)
CAPEX of BESS	Battery	1684.2	1684.2	1684.2	1684.2
	Converter	3300.0	3300.0	3300.0	3761.3
	BOS	1495.3	1495.3	1495.3	1633.7
OPEX of BESS		445.0	445.0	445.0	486.2
CAPEX of Connection	Application	46.2	26.1	26.1	26.1
	NAoR	6240.0	0.0	0.0	0.0
OPEX of Connection	NAoR	506.6	0.0	0.0	0.0
	δTNUoS	122.9	157.9	157.9	157.9
	δBSUoS	96.2	50.7	76.4	73.2
Total Cost		13,936.4	7159.4	7184.9	7822.6
Revenue related to EFR ($R_{EFR}^{AF} + R_{EFR}^{IMB}$)		14,186.4	14,139.1	14,098.9	14,155.9
Revenue related to Wind Generation (δR_{WG})		0	−169.8	278.7	11,986.1
Total Revenue		14,186.4	13,969.4	14,377.6	26,142.0
Final NPV		250.0	6809.9	7192.8	18,319.4

Though positive final NPVs are achieved in the case studies above, the variations of key financial elements such as the EFR tendered price $\mathcal{P}_{EFR}$ and the annual return rate d will translate in the uncertainties of the system profitability, which in turn affect the optimisation of the BESS capacity and SOC-related strategy variables. To examine the impacts of $\mathcal{P}_{EFR}$ and d on the system profitability, the final NPVs achieved in Scenarios (iii) and (iv) based on the optimisation variables in Table 3 combined with $\mathcal{P}_{EFR}$ varying between GBP 5/MW of EFR/hr and GBP 9.44/MW of EFR/hr and d ranging from 8% to 12% are plotted in Figure 12. The system profitability is shown to be largely influenced by $\mathcal{P}_{EFR}$, especially in Scenario (iii) where the final NPV reduces to about GBP 45k only given GBP 5/MW of EFR/hr and an annual return of 12%. This means that the updated financial elements could change the trade-off between the BESS investment and its associated benefits in terms of the EFR provision and the time shift of WG, driving the need of re-optimising the BESS size along with SOC-related strategy variables under new circumstances. The sensitivity of the optimsiation variables to some particular financial elements (e.g., d, $\mathcal{P}_{EFR}$, renewables subsidy, and BESS costs per MW and MWh) involved in the PSO process should be assessed in further work to provide a basis for the determination of the BESS size under the uncertainties of financial elements.

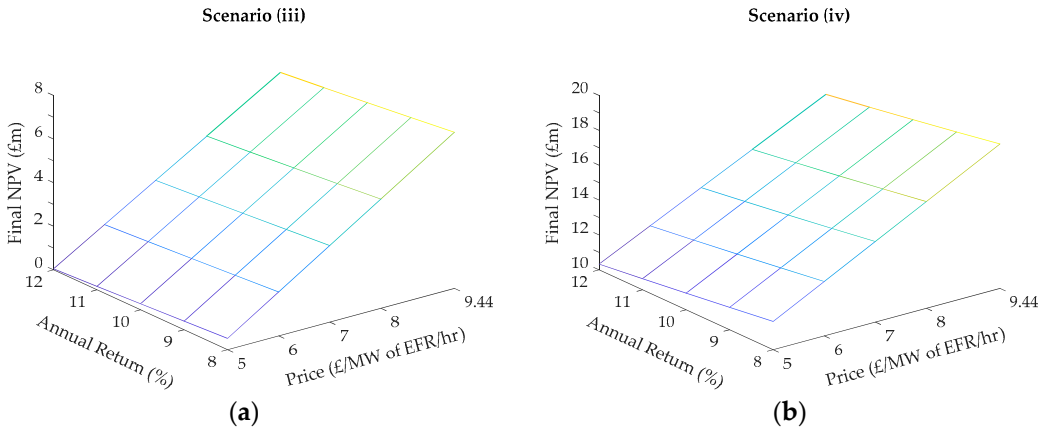

(**a**) (**b**)

Figure 12. The final NPVs (million GBP) achieved in (**a**) Scenario (iii) and (**b**) Scenario (iv) based on the optimisation variables in Table 3 given EFR tendered prices between GBP 5/MW of EFR/hr and GBP 9.44/MW of EFR/hr and annual return rates between 8% and 12%.

5. Conclusions and Future Work

With the fast development of battery technologies, co-locating battery energy storage systems (BESS) with renewable power plants has been receiving great attention in terms of the stacking of multiple revenue streams. Based on the UK's perspective, this paper has simulated the wind + BESS system under different coordination strategies where the BESS uses the existing connection point of the wind farm (WF) to provide enhanced frequency response (EFR) service and, given the placement of a converter between the BESS and the WF, realises the time shift of wind generation (WG). Then, a particle swarm optimisation algorithm was used in conjunction with the wind + BESS model to determine the BESS size and the state of charge (SOC)-related strategy variables that maximise the final net present value (NPV) of the co-located system at the end of a 4-year EFR contract.

Though the BESS size optimisation is case-dependent, the BESS supporting the maximum contract EFR capacity of 50 MW is recommended in the simulation given the average price of the first EFR tender. The study shows that the optimised wind + BESS systems achieve a slightly lower revenue from EFR (i.e., a reduction within 1%) than a stand-alone BESS, however, the avoidance of charges for new assets or reinforcements needed for an independent connection greatly increases the project profitability. In addition, the adjustment of EFR delivery within the envelopes to alleviate WG curtailment has increased the WG-related revenue. When a converter is placed between WF and BESS to assist in their energy exchange, the revenues given by the time shift of WG lead to the highest final NPV among different scenarios modelled here in spite of the increased project costs.

Building on the present work, the simulation model should be extended further to enable other revenue streams such as Dynamic Low High [13] and black start [8]. Furthermore, the profitability of using different battery technologies will be compared by modelling the characteristics of each technology including its price, charging profile and degradation. Moreover, the sensitivity of the optimal BESS size to key financial elements should be evaluated. In addition, the configuration and coordination strategies of co-located systems will be developed further to adapt for the stacking of various revenue streams.

Author Contributions: Conceptualization, G.Z. and D.C.-G.; methodology, software and data curation, F.F., G.Z. and D.C.-G.; validation, formal analysis and investigation, F.F., G.Z., D.C.-G. and J.N.; writing—original draft preparation and visualization, F.F. and G.Z.; writing—review and editing, D.C.-G. and J.N.; supervision, D.C.-G., G.B., O.A.-L., J.N. and A.M.; project administration and funding acquisition, D.C.-G. and A.M. All authors have read and agreed to the published version of the manuscript.

Funding: This work was conducted as part of the research programme of the Electrical Infrastructure Research Hub in collaboration with the Offshore Renewable Energy Catapult and also funded by the EPSRC EP/K503861/1 "Impact Acceleration Account—University of Strathclyde".

Data Availability Statement: The data used in this study are openly available in references [40], [48], and [49].

Conflicts of Interest: The authors declare no conflict of interest.

Nomenclature

Enhanced Frequency Response (EFR)

L	Lower EFR envelope
H	Higher EFR envelope
P_{EFR}^{cap}	Contracted EFR power capacity
P_{EFR}^{NPE}	EFR delivery in NPE strategy
P_{EFR}^{ENPE}	EFR delivery in ENPE strategy
P_{EFR}^{PE}	EFR delivery in PE strategy
$\bar{P}_{EFR}^{PE}$	Average EFR delivery in PE strategy in a settlement period (SP)
$\bar{P}_{EFR}^{ins}$	Average EFR delivery inside the deadband in a SP
SPM	Service performance measure
$ASPM$	Average SPM over 12 months
AF	Availability factor
Δt	Time step length in simulation

Wind Farm (WF)

P_{WF}^{tot}	Available wind power
P_{WF}^{sell}	Wind power flowing to WF meter
P_{WF}^{curt}	Wind power curtailment
P_{WF}^{store}	Wind power flowing to BESS
P_{CON}	Ampacity of connection point
$\delta\bar{P}_{WF}^{sell}$	Average difference in power flow across WF meter between a wind + BESS system and a single WF in a SP

Battery Energy Storage System (BESS)

P_{BESS}^{rated}	Power capacity of BESS
C_{BESS}^{rated}	Energy capacity of BESS
P_{AdC}^{r}	Power capacity of the converter (AdC) between BESS and WF
P_{BESS}^{dis}	Discharge rate of BESS
P_{BESS}^{ch}	Charge rate of BESS
$\underline{P}_{BESS}^{ch}$	State of change (SOC)-related limit on charge rate of BESS
P_{BESS}^{sell}	BESS power flowing to WF meter
η_{dis}	Discharging efficiency of BESS
η_{ch}	Charging efficiency of BESS
η_{AdC}^{D2A}	DC-to-AC efficiency of AdC
η_{AdC}^{A2D}	AC-to-DC efficiency of AdC
SOC_{min}	Minimum allowable SOC level
SOC_{max}	Maximum allowable SOC level
SOC_o	Initial SOC of BESS in Δt
SOC_{new}	Final SOC of BESS in Δt
SOC_t^{tem}	Temporary SOC after delivery of P_{EFR}^{NPE} in ENPE strategy
SOC_t^{PE}	Temporary SOC after delivery of P_{EFR}^{PE} in PE strategy
SOC_{l1}, SOC_{l2}, SOC_{h2}, SOC_{h1}, SOC_r, SOC_{ld}, SOC_{hc}	SOC-related strategy variables

Battery Degradation Model

$f_d(\cdot)$	BESS degradation function
$f_c(\cdot)$	Cycle ageing function
$f_t(\cdot)$	Calendar ageing function
td	Time period for degradation update

N_c	Number of cycles over td
ε_i	Depth of discharge in a cycle
$T_{c,i}$	Cell temperature in a cycle
$\bar{T}_c$	Average cell temperature over td
σ_i	Average SOC in a cycle
$\bar{\sigma}$	Average SOC over td
α_{SEI}	Coefficient in the solid electrolyte interphase (SEI) model
β_{SEI}	Coefficient in the SEI model
RC_D	Remaining capacity of BESS at the end of the D-days
RC_{end}	Remaining capacity of BESS at the end of the 4-years

Revenue and Cost Calculation

$CAPEX_{BESS}$	CAPEX of BESS
$CAPEX_{CON}$	CAPEX of BESS connection
$OPEX_{BESS,m}$	Monthly OPEX of BESS
$\delta TNUoS$	Change of annual TNUoS charge
$\delta TNUoS_m$	Change of monthly TNUoS charge
$\delta BSUoS_{sp}$	Change of BSUoS charge in a SP
$\delta BSUoS_m$	Change of BSUoS charge in a month
$\delta R_{WG,sp}$	Revenue related to $\bar{P}_{WF}^{sell}$ in a SP
$\delta R_{WG,m}$	Revenue related to $\bar{P}_{WF}^{sell}$ in a month
$R_{EFR,sp}^{AF}$	EFR availability payment in a SP
$R_{EFR,m}^{AF}$	EFR availability payment in a month
$R_{EFR,sp}^{IMB}$	Energy imbalance charge related to $\bar{P}_{EFR}^{ins}$ in a SP
$R_{EFR,m}^{IMB}$	Energy imbalance charge related to $\bar{P}_{EFR}^{ins}$ in a month
NPV	Net present value
$\mathcal{P}_{EFR}$	EFR tendered price
$\mathcal{P}_{IMB}$	Energy imbalance price
$\mathcal{P}_{ROC}$	Renewables subsidy price under Renewables Obligation
m	Number of calendar months
d	Annual return rate

References

1. Renewable Energy Association. *Energy storage in the UK—An Overview*; Renewable Energy Association: London, UK, 2016.
2. Fan, F.; Xu, H.; Kockar, I. Utilisation of energy storage to improve distributed generation connections and network operation on Shetland Islands. In Proceedings of the 25th International Conference and Exhibition on Electricity Distribution, Madrid, Spain, 3–6 June 2019; pp. 1–5.
3. Li, C.; Zhou, H.; Li, J.; Dong, Z. Economic dispatching strategy of distributed energy storage for deferring substation expansion in the distribution network with distributed generation and electric vehicle. *J. Clean. Prod.* **2020**, *253*, 119862.
4. Greenwood, D.M.; Lim, K.Y.; Patsios, C.; Lyons, P.F.; Lim, Y.S.; Taylor, P.C. Frequency response services designed for energy storage. *Appl. Energy* **2017**, *203*, 115–127.
5. Gundogdu, B.; Nejad, S.; Gladwin, D.T.; Foster, M.P.; Stone, D.A. A battery energy management strategy for UK enhanced frequency response and triad avoidance. *IEEE Trans. Ind. Electron.* **2018**, *65*, 9509–9517.
6. Metz, D.; Saraiva, J.T. Use of battery storage systems for price arbitrage operations in the 15- and 60-min German intraday markets. *Electr. Power Syst. Res.* **2018**, *160*, 27–36.
7. Campos-Gaona, D.; Madariaga, A.; Zafar, J.; Anaya-Lara, O.; Burt, G. Techno-economic analysis of energy storage system for wind farms: The UK perspective. In Proceedings of the 2018 International Conference on Smart Energy Systems and Technologies, Sevilla, Spain, 10–12 September 2018.
8. Energy UK. Ancillary Services Report 2017. Available online: https://www.energy-uk.org.uk/publication.html?task=file.download&id=6138 (accessed on 24 March 2020).
9. National Grid Electricity System Operator (NGESO). Firm Frequency Response (FFR). Available online: https://www.nationalgrideso.com/balancing-services/frequency-response-services/firm-frequency-response-ffr (accessed on 25 March 2020).
10. NGESO. State of Charge Management Guidance for FFR Providers. Available online: https://www.nationalgrideso.com/sites/eso/files/documents/State%20of%20Charge%20management%20publication%20-%20EXT_0.pdf (accessed on 25 March 2020).

11. NGESO. Enhanced Frequency Response Market Information Report. Available online: https://www.nationalgrideso.com/sites/eso/files/documents/EFR%20Market%20Information%20Report%20v1.pdf (accessed on 7 February 2020).
12. NGESO. Response and Reserve Roadmap. Available online: https://www.nationalgrideso.com/document/157791/download (accessed on 25 March 2020).
13. NGESO. Phase 2 Auction Trial. Available online: https://www.nationalgrideso.com/balancing-services/frequency-response-services/frequency-auction-trial?technical-requirements (accessed on 25 March 2020).
14. Office of Gas and Electricity Markets (OFGEM). Guidance for Generators That Receive or Would Like to Receive Support under the Renewables Obligation (RO) Scheme. Available online: https://www.ofgem.gov.uk/system/files/docs/2019/04/ro_generator_guidance_apr19.pdf (accessed 28 February 2020).
15. Department for Business, Energy & Industrial Strategy. Policy Paper Contracts for Difference. Available online: https://www.gov.uk/government/publications/contracts-for-difference/contract-for-difference (accessed on 24 February 2020).
16. Ye, R.L.; Guo, Z.Z.; Liu, R.Y.; Liu, J.N. An optimal sizing method for energy storage system in wind farms based on analysis of wind power forecast error. *IOP Conf. Ser. Mater. Sci. Eng.* **2016**, *161*, 012085.
17. Korpaas, M.; Holen, A.T.; Hildrum, R. Operation and sizing of energy storage for wind power plants in a market system. *Int. J. Electr. Power Energy Syst.* **2003**, *25*, 599–606.
18. Michiorri, A.; Lugaro, J.; Siebert, N.; Girard, R.; Kariniotakis, G. Storage sizing for grid connected hybrid wind and storage power plants taking into account forecast errors autocorrelation. *Renew. Energy* **2018**, *117*, 380–392.
19. Liu, Y.; Du, W.; Xiao, L.; Wang, H.; Cao, J. A method for sizing energy storage system to increase wind penetration as limited by grid frequency deviations. *IEEE Trans. Power Syst.* **2016**, *31*, 729–737.
20. Mejía-Giraldo, D.; Velásquez-Gomez, G.; Muñoz-Galeano, N.; Cano-Quintero, J.B.; Lemos-Cano, S. A BESS sizing strategy for primary frequency regulation support of solar photovoltaic plants. *Energies* **2019**, *12*, 317.
21. Munoz-Vaca, S.; Patsios, C.; Taylor, P. Enhancing frequency response of wind farms using hybrid energy storage systems. In Proceedings of the 2016 IEEE International Conference on Renewable Energy Research and Applications, Birmingham, UK, 20–23 November 2016.
22. NGESO. Enhanced Frequency Response Invitation to Tender for Pre-Qualified Parties. Available online: https://www.nationalgrideso.com/document/101541/download (accessed on 12 February 2020).
23. Cho, I.H.; Lee, P.Y.; Kim, J.H. Analysis of the effect of the variable charging current control method on cycle life of Li-ion batteries. *Energies* **2019**. *12*, 3023.
24. Dixon, J.; Andersen, P.B.; Bell, K.; Træholt, C. On the ease of being green: An investigation of the inconvenience of electric vehicle charging. *Appl. Energy* **2020**, *258*, 114090.
25. Wei, Z.; Leng, F.; He, Z.; Zhang, W.; Li, K. Online state of charge and state of health estimation for a Lithium-Ion battery based on a data-model fusion method. *Energies* **2018**, *11*, 1810.
26. Canevese, D.; Cirio, D.; Gatti, A.; Rapizza, M.; Micolano, E.M.; Pellegrino, L. Simulation of enhanced frequency response by battery storage systems: The UK versus the continental Europe system. In Proceedings of the 2017 IEEE International Conference on Environment and Electrical Engineering and 2017 IEEE Industrial and Commercial Power Systems Europe, Milan, Italy, 6–9 June 2017.
27. Johnston, L.; Díaz-González, F.; Gomis-Bellmunt, O.; Corchero-García, C.; Cruz-Zambrano, M. Methodology for the economic optimisation of energy storage systems for frequency support in wind power plants. *Appl. Energy* **2015**, *137*, 660–669.
28. Wu, J.; Wei, Z.; Liu, K.; Quan, Z.; Li, Y. Battery-involved energy management for hybrid electric bus based on expert-assistance deep deterministic policy gradient algorithm. *IEEE Trans. Veh. Technol.* **2020**, *69*, 12786-12796.
29. Wu, J.; Wei, Z.; Li, W.; Wang, Y.; Li, Y.; Sauer, D.U. Battery thermal- and health-constrained energy management for hybrid electric bus based on soft actor-critic DRL algorithm. *IEEE Trans. Ind. Inform.* **2020**, doi:10.1109/TII.2020.3014599.
30. Xu, B.; Oudalov, A.; Ulbig, A.; Andersson, G.; Kirschen, D.S. Modeling of Lithium-Ion battery degradation for cell life assessment. *IEEE Trans. Smart Grid* **2018**, *9*, 1131–1140.
31. Lee, Y.L.; Tjhung, T. Rainflow cycle counting techniques. In *Metal Fatigue Analysis in Handbook: Practical Problem-Solving Techniques for Computer-Aided Engineering*, 1st ed.; Lee, Y.L., Barkey, M.E., Kang, H.T., Eds.; Butterworth-Heinemann: Waltham, MA, USA, 2012; Volume 3, pp. 89–114.
32. NGESO. Enhanced Frequency Response Frequently Asked Questions. Available online: https://www.nationalgrid.com/sites/default/files/documents/Enhanced%20Frequency%20Response%20FAQs%20v5.0_.pdf (accessed on 24 February 2020).
33. ELEXON. Imbalance Pricing Guidance: A guide to Electricity Imbalance Pricing in Great Britain. Available online: https://www.elexon.co.uk/documents/training-guidance/bsc-guidance-notes/imbalance-pricing/ (accessed on 24 February 2020).
34. OFGEM. Renewable Obligation (RO) Buy-Out Price and Mutualisation Ceilings for 2020–21. Available online: https://www.ofgem.gov.uk/publications-and-updates/renewables-obligation-ro-buy-out-price-and-mutualisation-ceilings-2020-21 (accessed on 28 February 2020).
35. Interim Levy Rate Calculation for Quarterly Obligation Period from 01 January 2020–31 March 2020. Available online: https://sofm.lowcarboncontracts.uk/interimratecalculation?tab=%22Definition%22#. (accessed on 24 February 2020).
36. Jülch, V. Comparison of electricity storage options using levelized cost of storage (LCOS) method. *Appl. Energy* **2016**, *183*, 1594–1606.
37. NGESO. Introduction to Co-Location. Available online: https://www.nationalgrideso.com/document/139786/download (accessed on 7 February 2020).

38. NGESO. Application Fee Calculator 19_20_0. Available online: https://www.nationalgrideso.com/document/154976/download (accessed on 24 February 2020).
39. NGESO. TNUoS Guidance for Generators. Available online: https://www.nationalgrideso.com/document/138046/download (accessed on 24 February 2020).
40. NGESO. Balancing Services Use of System (BSUoS) Charges. Available online: https://www.nationalgrideso.com/charging/balancing-services-use-system-bsuos-charges (accessed on 24 February 2020).
41. National Grid. Cost Estimator. Available online: https://www.nationalgridet.com/get-connected/cost-estimator (accessed on 24 February 2020).
42. Final TNUoS Tariffs for 2019/20. Available online: https://www.nationalgrideso.com/document/137351/download (accessed on 24 February 2020).
43. Žižlavský, O. Net present value approach: Method for economic assessment of innovation projects. *Procedia Soc. Behav. Sci.* **2014**, *156*, 506–512.
44. Kennedy, J.; Eberhart, R. Particle swarm optimization. In Proceedings of the International Conference on Neural Networks, Perth, Australia, 27 November–1 December 1995; pp. 1942–1948.
45. The MathWorks, Inc. Particle Swarm Optimization, Particleswarm. Available online: https://www.mathworks.com/help/gads/particleswarm.html (accessed on 24 February 2020).
46. Lee, K.Y.; Park, J.B. Application of particle swarm optimization to economic dispatch problem: Advantages and disadvantages. In Proceedings of the 2006 IEEE PES Power Systems Conference and Exposition, Atlanta, GA, USA, 29 October–1 November 2006.
47. National Grid, Round 3 Offshore Wind Farm Connection Study—Version 1.0. Available online: https://www.waveandtidalknowledgenetwork.com/wp-content/uploads/legacy-files/00883.pdf (accessed on 24 February 2020).
48. ELEXON. System Sell & System Buy Prices. Available online: https://www.bmreports.com/bmrs/?q=balancing/systemsellbuyprices (accessed on 7 February 2020).
49. NGESO. Historic Frequency Data. Available online: https://www.nationalgrideso.com/balancing-services/frequency-response-services/historic-frequency-data (accessed on 7 February 2020).
50. MATLAB Release 2018b, The MathWorks, Inc., Massachusetts, USA.
51. Jamian, J.J.; Abdullah, M.N.; Mokhils, H.; Mustafa, M.W.; Bakar, A.H.A. Global particle swarm optimization for high dimension numerical functions analysis. *J. Appl. Math.* **2014**, *2014*, 329193.